PROCEEDINGS OF SCIENCE

arXiv:0708.2613v1 [nucl-th] 20 Aug 2007

Pion freeze-out through HBT correlation in HICs from AGS/FAIR to RHIC energies

Qingfeng Li[*†]
Frankfurt Institute for Advanced Studies (FIAS), Frankfurt
E-mail: liqf@fias.uni-frankfurt.de; liqfer@gmail.com

In this talk we present the results of two-pion HBT correlation at freeze-out in heavy ion collisions (HICs) from AGS to RHIC energies. The UrQMD hadron-string transport model as well as the CRAB analyzing program are adopted. Based on the cascade mode, in general, the calculations are satisfying and well in line with the experimental data although discrepancies are not negligible. Such as: I), the HBT time-related puzzle exists at all energies. II), at low AGS energies, the calculated volume as well as the mean free path of pion source at freeze-out are lower than data. It implies that a better description of interactions of particles at early stage of HICs is required.

Critical Point and Onset of Deconfinement 4th International Workshop
July 9-13 2007
GSI Darmstadt,Germany

[*]Speaker.
[†]In collaboration with Marcus Bleicher and Horst Stöcker.

© Copyright owned by the author(s) under the terms of the Creative Commons Attribution-NonCommercial-ShareAlike Licence.

1. Introduction

For discovering the theoretically predicted quark gluon plasma (QGP) the heavy ions have been collided with nucleon-nucleon center-of-mass energies from less than $\sqrt{s} \sim 2.5$ GeV (SIS/FAIR energy regime), $2.5-20$ GeV (AGS/FAIR and SPS) up to $20-200$ GeV (RHIC). Indeed, there are some signals - such as charmonium suppression, relative strangeness enhancement, etc. - of the (phase) transition to the deconfined phase have been observed in heavy ion collisions (HICs) at SPS energies [1, 2, 3, 4]. Additional information about the space-time structure of the particle emission source (the region of homogeneity) can be extracted by Femtoscopy [5] or namely Hanbury-Brown-Twiss interferometry (HBT) [6]. It is supposed that non-trivial structures in the excitation function of HBT quantities should be present at the energy threshold for the onset of QGP formation [7]. Unfortunately, so far the excitation functions of the HBT quantities have not shown any *obvious* discontinuities within the large span of explored beam energies [5, 8, 9, 10, 11, 12, 13, 14, 15, 16, 17, 18, 19].

A comprehensive theoretical investigation on the excitation function of the HBT parameters is thus highly required but still absent so far [5]. Recently, based on the UrQMD hadron-string transport model [20, 21, 22] and the CRAB [23, 24] analyzing program, we investigated the beam energy, transverse momentum, system-size, centrality, and rapidity dependence of the HBT parameters R_L, R_O, R_S (dubbed as HBT radii or Pratt radii), and the cross term R_{OL} of pion source [25, 26, 27, 28]. In general, the calculations are satisfying and well in line with the experimental data although discrepancies are not negligible. Such as, I), the calculated R_L and R_S values for Au+Au collisions at low AGS energies are visibly smaller than the data if the default UrQMD version 2.2 (cascade mode) is adopted. II), the HBT-'puzzle' with respect to the 'duration time' of the pion source, is present at all energies.

In this presentation, we show the beam energy and transverse momentum dependence of the pion HBT radii, as well as some other radius-related quantities such as the "duration-time" related quantity $\sqrt{R_O^2 - R_S^2}$ (and the R_O/R_S ratio), the freeze-out volume V_f, and the mean free path λ_f of pions at freeze-out. The standard UrQMD v2.2 in cascade mode is employed firstly to serve as a benchmark, then we find that the HBT time-related puzzle can be better understood with the consideration of a potential interaction.

2. UrQMD transport model

The UrQMD model is based on analogous principles as the Quantum Molecular Dynamics (QMD) [29, 30] and the RQMD [31] transport models. Similar to QMD, hadrons are represented by Gaussian wave packets in phase space, and the phase space of hadron i is propagated according to Hamilton's equation of motion: $\dot{\mathbf{r}}_i = \frac{\partial H}{\partial \mathbf{p}_i}$ and $\dot{\mathbf{p}}_i = -\frac{\partial H}{\partial \mathbf{r}_i}$. Here $\mathbf{r}$ and $\mathbf{p}$ are the coordinate and momentum of hadron i. The Hamiltonian H consists of the kinetic energy T and the effective two-body interaction potential energy U. In the standard version of UrQMD model [20, 21], the potential energies include the two-body and three-body (which can be approximately written in the form of two-body interaction) Skyrme- (also called as the density dependent terms), Yukawa-, Coulomb-, and (optional) Pauli-terms as a base. Recently, in order to be more successfully applied in the intermediate energy region ($E_b \lesssim 2$A GeV), more potentials are considered into the

model [32], those are, the density-dependent symmetry potential (essential for isospin-asymmetric reactions at intermediate and low energies) and the phenomenologically momentum-dependent interaction. We have found that the experimental pion and proton directed and elliptic flows from HICs with beam energies from $\sim$ 100A MeV to 2A GeV can be well described with the potentials [33]. At higher energies, i.e., AGS/FAIR, the Yukawa-, Pauli-, and symmetry- potentials of baryons become negligible, while the Skyrme- and the momentum-dependent parts of potentials still influence the whole dynamical process of HICs. For example, in Ref. [34], with the help of a mean field from RQMD/S [35] and a Jet AA Microscopic Transportation Model (JAM) it has been found that the momentum dependence in the nuclear mean field is important for the understanding of the proton collective flows at AGS and SPS energies.

In the latter part of the presentation, we will also show the importance of the mean field on the HBT time related puzzle. We adopt the soft equation of state (EoS) with momentum dependence (SM-EoS) which is same as that in Ref. [34]. Furthermore, as in [34], the relativistic effects on the relative distance $\mathbf{r}_{ij} = \mathbf{r}_i - \mathbf{r}_j$ and and the relative momentum $\mathbf{p}_{ij} = \mathbf{p}_i - \mathbf{p}_j$ (Lorentz transformation) employed in the two-body potentials are considered:

$$\tilde{\mathbf{r}}_{\mathbf{ij}}^{\mathbf{2}} = \mathbf{r}_{ij}^2 + \gamma_{ij}^2 (\mathbf{r}_{ij} \cdot \beta_{ij})^2; \tag{2.1}$$

$$\tilde{\mathbf{p}}_{\mathbf{ij}}^{\mathbf{2}} = \mathbf{p}_{ij}^2 - (E_i - E_j)^2 + \gamma_{ij}^2 (\frac{m_i^2 - m_j^2}{E_i + E_j})^2. \tag{2.2}$$

In Eqs. 2.1 and 2.2 the velocity-factor β_{ij} and the corresponding γ-factor of i and j particles are defined as

$$\beta_{ij} = \frac{\mathbf{p}_i + \mathbf{p}_j}{E_i + E_j}, \text{ and } \gamma_{ij} = \frac{1}{\sqrt{1 - \beta_{ij}^2}}. \tag{2.3}$$

Similar to RQMD, the collision term of the UrQMD model treats 55 different baryon species (including nucleon-, delta- and hyperon- resonances with masses up to 2.25 GeV) and 32 different meson species, including (strange) meson resonances with masses up to 2.0 GeV as tabulated in the PDG [36], as well as the corresponding anti-particles, i.e. full baryon/antibaryon symmetry is included. Isospin is explicitly treated as well. For hadronic continuum excitations a string model is used. Starting from the version 2.0, the PYTHIA is incorporated into UrQMD in order to investigate the jet production and fragmentation at RHIC energies [22].

3. Analyzing process

To calculate the two-particle correlator, the CRAB program is based on the formula:

$$C(\mathbf{k}, \mathbf{q}) = \frac{\int d^4x_1 d^4x_2 g(x_1, \mathbf{p_1}) g(x_2, \mathbf{p_2}) |\phi(\mathbf{q}, \mathbf{r})|^2}{\int d^4x_1 g(x_1, \mathbf{p_1}) \int d^4x_2 g(x_2, \mathbf{p_2})}. \tag{3.1}$$

Here $g(x, \mathbf{p})$ is the probability for emitting a particle with momentum $\mathbf{p}$ from the space-time point $x = (\mathbf{r}, t)$. $\phi(\mathbf{q}, \mathbf{r})$ is the relative two-particle wave function with $\mathbf{r}$ being their relative position. $\mathbf{q} = \mathbf{p_2} - \mathbf{p_1}$ and $\mathbf{k} = (\mathbf{p}_1 + \mathbf{p}_2)/2$ are the relative momentum and the average momentum of the two particles. Due to the underlying quantum statistics, this correlator can be fitted approximately by

a Gaussian form. Using Pratt's three-dimensional convention (the LCMS system), the correlation function in Gaussian form reads

$$C(q_O,q_S,q_L) = 1+\lambda\exp(-R_L^2q_L^2 - R_O^2q_O^2 - R_S^2q_S^2 - 2R_{OL}^2q_Oq_L). \tag{3.2}$$

Here q_i and R_i are the components of the pair momentum difference $\mathbf{q}$ and the homogeneity length (HBT radii) in the i direction, respectively. The pre-factor λ is the incoherence parameter and lies between 0 (complete coherence) and 1 (complete incoherence) in realistic HICs. The term R_{OL}^2 is called cross-term and vanishes at mid-rapidity for symmetric systems, while it deviates from zero at large rapidities [37, 27].

We compare our calculations of the Pratt parameters (at midrapidity) of the pion source with experimental data for the following central collisions of heavy nuclei:

1. Au+Au at the AGS beam energies $E_b = 2$, 4, 6, and 8A GeV ($< 11\%$ of the total cross section σ_T), a rapidity cut $|Y_{cm}| < 0.5$ ($Y_{cm} = \frac{1}{2}\log(\frac{E_{cm}+p_\parallel}{E_{cm}-p_\parallel})$, E_{cm} and $p_\parallel$ are the energy and longitudinal momentum of the pion meson in the center-of-mass system) is employed. The experimental (E895) data are taken from [9].

2. Au+Au at the AGS beam energy 11.6A GeV (the $< 5\%$ most central collisions), a rapidity cut $|Y_{cm}| < 0.5$ is employed. The experimental (E802) data are taken from [10].

3. Pb+Pb at the SPS beam energies $E_b = 20$, 30, 40, 80, and 160A GeV ($< 7.2\%\sigma_T$ of most central collisions), a pion-pair rapidity cut $|Y_{\pi\pi}| < 0.5$ ($Y_{\pi\pi} = \frac{1}{2}\log(\frac{E_1+E_2+p_{\parallel 1}+p_{\parallel 2}}{E_1+E_2-p_{\parallel 1}-p_{\parallel 2}})$ is the pair rapidity with pion energies E_1 and E_2 and longitudinal momenta $p_{\parallel 1}$ and $p_{\parallel 2}$ in the center of mass system) is employed. The experimental (NA49) data are taken from [11, 12].

4. Pb+Au at the SPS beam energies $E_b = 40$, 80, and 160A GeV (the $< 5\%$ most central collisions), the pion-pair rapidity cut $Y_{\pi\pi} = -0.25 \sim 0.25$, $-0.5 \sim 0$, and $-1.0 \sim -0.5$ are chosen. The experimental (CERES) data are taken from [13].

5. Au+Au at the RHIC energies $\sqrt{s_{NN}} = 30$ ($< 15\%\sigma_T$), 62.4 ($< 15\%\sigma_T$), 130 ($< 10\%\sigma_T$), and 200 GeV ($< 5\%\sigma_T$). Here a pseudo-rapidity cut $|\eta_{cm}| < 0.5$ ($\eta_{cm} = \frac{1}{2}\log(\frac{p+p_\parallel}{p-p_\parallel})$, ($p$ is the momentum of the pion) is employed. The experimental (PHOBOS, STAR, and PHENIX) data are taken from [15, 16, 18, 14, 17].

4. The HBT radii at AGS, SPS, and RHIC energies

Fig. 1 shows the k_T ($\mathbf{k}_T = (\mathbf{p}_{1T}+\mathbf{p}_{2T})/2$) dependent HBT radii R_L (top), R_O (middle), and R_S (bottom) of the $\pi^-\pi^-$-pair for AGS energies 2, 4, 6, 8, and 11.6A GeV (from left to right). The cascade mode is employed. We notice that the radii R_L and R_S are somewhat smaller than the data especially at lower beam energies, if a constant width for resonances (lines with diamonds) is used. Fig. 1 also includes the results with the mass dependent lifetime of resonances (lines with triangles). With this treatment, the resonances with their small invariant masses decay later and hence the expanded fireball becomes larger as compared to the standard (mass independent) treatment. At large k_T as well higher beam energies, this effect is reduced. It is interesting to see that the result with a mass-dependent treatment of resonance lifetimes can matches the data much

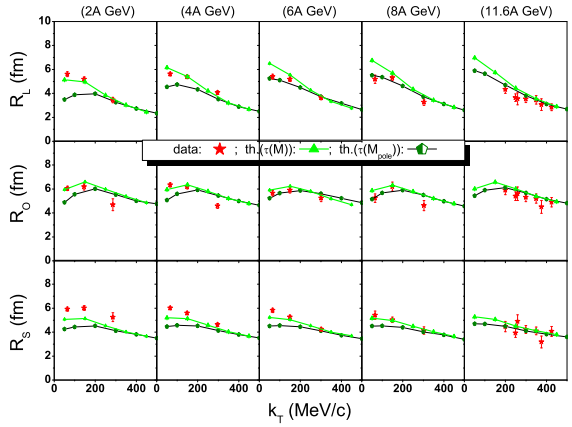

Figure 1: Transverse momentum k_T dependence of the HBT-radii R_L, R_O, and R_S at AGS energies. The calculated results with and without considering the mass dependence of resonance lifetimes are demonstrated. Experimental data are shown [9, 10] with scattered stars.

better in the AGS energy region. It is also seen that this mass-dependence has almost no effect on the ratio between R_O and R_S values.

In Figs. 2 and 3 we show the k_T dependence of the HBT- radii R_L (top plots), R_O (middle plots), and R_S (bottom plots) at SPS energies. In Fig. 2 the results are compared with preliminary NA49 data [12]. In Fig. 3 the results are compared with CERES data [13]. Furthermore, the $\pi^- - \pi^-$ correlations are calculated in Fig. 2 while the two-charged-pion correlations (including two-π^- and two-π^+ mesons) are calculated in Fig. 3. Firstly, it is very interesting to see that the present calculations can reproduce the k_T-dependence of HBT radii R_L and R_S fairly well. Only at small k_T, the calculated R_L and R_S values are seen up to 25% lower than data. While for the R_O values, the calculations are shown larger than both NA49 and CERES data especially at relatively large k_T. By comparing the NA49 data with the CERES data for central Pb+Pb ($\sigma/\sigma_T < 7.2\%$) and central Pb+Au ($\sigma/\sigma_T < 5\%$) collisions, one observes that the CERES R_O data are somewhat smaller than the recent published NA49 data [12] especially at large k_T and low beam energy $E_b = 40$A GeV although the recent NA49 data at large k_T have already been driven down visibly when comparing with those preliminary data in the previous publication [11]. The origin of the difference between NA49 and CERES data is still not quite clear. At 160 A GeV (shown in Fig. 2) the HBT radii are also calculated by adopting zero formation time for strings ($\tau_s = 0$ fm/c). As a result, the k_T-dependence of the HBT radii becomes steeper, and the values of R_S increase and approach the calculated R_O values. It should be noted that, although a shorter formation time is apt to explain the "HBT-puzzle", as well the elliptic flow, the absolute values of HBT-radii are not well in line with data.

Fig. 4 gives the k_T dependence of the Pratt-radii R_L (left plots), R_O (middle plots), and R_S (right plots) at RHIC energies. Both the absolute values and the decrease of the Pratt-radii R_L and R_S with transverse momentum is reproduced by the present model calculations very well. Here, it is also seen that the calculated k_T-dependence of R_S is somewhat flatter than that of R_L, which implies that flow effect on the k_T-dependence of the Pratt-radii is still important. Besides the flow effect, the surface-like emission charactistic of microscopic models should play significantly role on HBT parameters as well because also other Cascade/Boltzmann model-calculations (see e.g., the RQMD [9, 5], the HRM [38], and the AMPT [39]) can reproduce the k_T dependence of Pratt

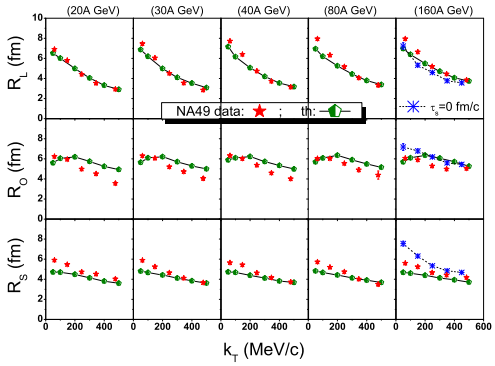

Figure 2: k_T dependence of the Pratt-radii at SPS energies. Preliminary NA49 data are taken from [12]. At $E_b = 160$A GeV the calculation results of the HBT-radii with a vanishing formation time for strings are also presented.

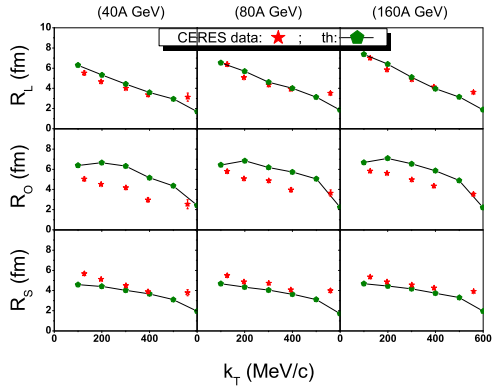

Figure 3: k_T dependence of the Pratt-radii at SPS energies. CERES data are taken from [13].

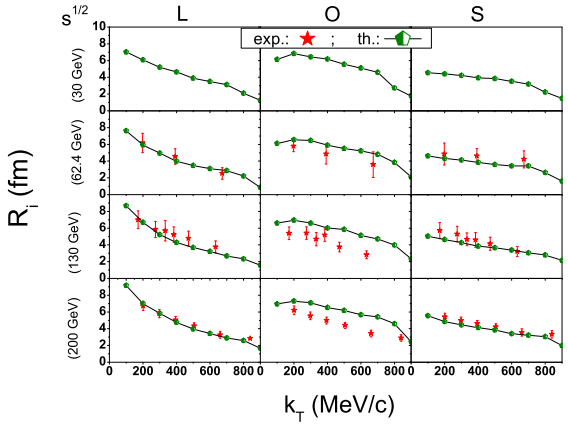

Figure 4: k_T dependence of the Pratt-radii R_L, R_O, and R_S at RHIC energies. Experimental data are shown [15, 16, 18, 14, 17] at $\sqrt{s_{NN}} = 62.4$, 130, and 200 GeV.

radii (almost) equally well. The UrQMD calculations of R_L and R_S reproduce the experimental data well within the error bars, while the calculated R_O's are also larger than the experimental data — the R_O is about 25% too large.

5. Excitation function of the V_f, the λ_f, and the $\sqrt{R_O^2 - R_S^2}$ (and R_O/R_S) of pions

Fig. 5 (a) shows the excitation function of the pion source volume V_f at freeze-out, calculated as [40] $V_f = (2\pi)^{\frac{3}{2}} R_L R_S^2$. The calculations with default cascade mode are shown at $k_T = 100 \pm 50$ MeV (full line) and 200 ± 50 MeV$/c$ (dotted line), respectively. The gray areas between the two lines are shown for better visibility. The data are at $k_T \sim 150$MeV$/c$ for AGS-E895 and SPS-NA49, at $k_T \sim 170$MeV$/c$ for reaction at $\sqrt{s_{NN}} = 130$ GeV, at $k_T \sim 200$MeV$/c$ for reactions at AGS-E802, SPS-CERES, and $\sqrt{s_{NN}} = 62.4, 200$ GeV. Since the experimental data from NA49 [11, 12]

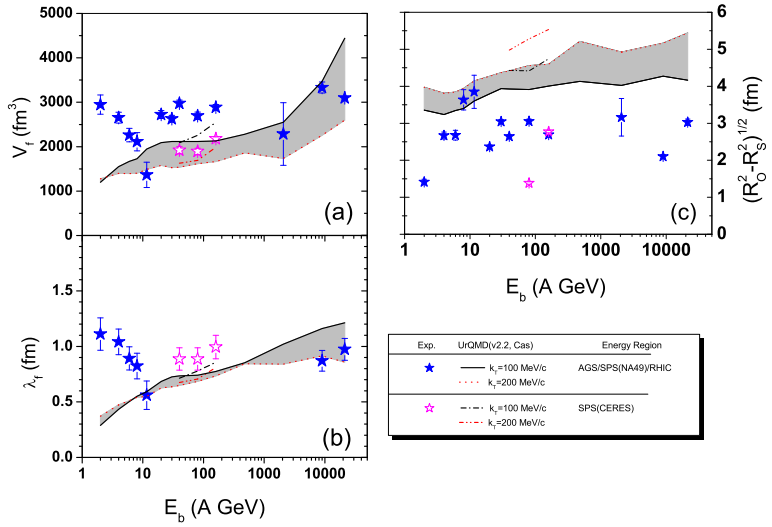

Figure 5: (a): Excitation function of the V_f at transverse momenta between $k_T =$ 100MeV and 200MeV (gray area), compared with data in this k_T-region. (b): Excitation function of the λ_f of pions at freeze-out. (c): Excitation function of the duration-time related quantity $\sqrt{R_O^2 - R_S^2}$.

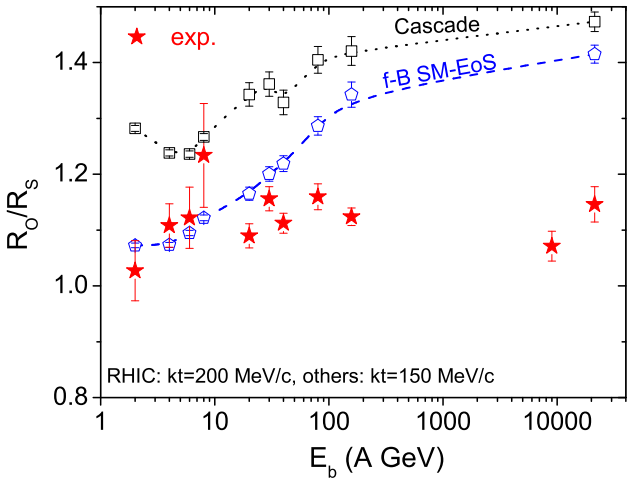

Figure 6: Excitation function of the R_O/R_S ratio at small k_T. The data are indicated by solid stars. The dotted lines with open rectangles are results under cascade mode, the dashed lines with open diamonds represent the calculations with potentials of formed baryons.

and from CERES [13] collaborations overlap at beam energies 40, 80, and 160A GeV, we show the calculations and data with respect to CERES energies separately as dashed-dotted lines and open symbols. Fig. 5 (a) shows clearly that the UrQMD cascade calculations do provide a reasonable freeze-out volume for the pion source at RHIC energies. At SPS energies, the agreement is fine with CERES data while it slightly underpredicts those of NA49. Towards even lower energies, the model underpredicts the measured freeze-out volume due to the omission of the strong interaction potential and other in-medium effects. E.g. at $E_b = 2A$ GeV, the measured V_f is about $2-3$ times larger than calculated value. As stated in Fig. 1, a mass-dependent lifetime of resonances accounts for an improvement of the HBT-radii at small k_T and hence reproduce the data better.

The mean free path λ_f of the pions at freeze-out is expressed as [40]

$$\lambda_f = \frac{V_f}{N\sigma} = \frac{V_f}{N_N\sigma_{\pi N} + N_\pi\sigma_{\pi\pi}}. \tag{5.1}$$

with the averaged pion-nucleon cross section $\sigma_{N\pi} = 72$ mb and the averaged pion-pion cross section $\sigma_{\pi\pi} = 13$ mb (Note that within the present model calculations these values are slightly energy dependent. However, here we have adopted the explicit numbers from Ref. [40] to compare to the results presented there). The nucleon and pion multiplicities N_N and N_π are calculated as

$$N_{N,\pi} = y_{th} \cdot \sqrt{2\pi} \cdot \frac{dN_{nucleons,pions}}{dy} \mid_{y_{mid}}. \tag{5.2}$$

using the assumption of a thermal equilibrated system at freeze-out with a temperature $T_f = 120$ MeV. Here, y_{th} is the estimated thermal homogeneity scale in rapidity at a certain k_T and T_f, and is given by the expressions: $y_{th} = \mathrm{arctanh}(\langle\beta_{th}\rangle)$, with $\langle\beta_{th}\rangle = \sqrt{1+\langle\gamma\rangle^2}/\langle\gamma\rangle$ and $\langle\gamma\rangle = 1 + 1/3\,(K_1(m_T/T_f)/K_2(m_T/T_f) - 1) + T_f/m_T$. Here $K_n(z)$ is the modified Bessel function of order n and $m_T = \sqrt{m_\pi^2 + k_T^2}$. $dN/dy|_{y_{mid}}$ is the rapidity density of pion (nucleons) at mid-rapidity. Recent calculations using the present UrQMD transport model [22] have shown that the calculated pion and nucleon yields are reasonably in agreement with data.

Fig. 5 (b) shows the excitation function of λ_f of pions at freeze-out. The experimental value for λ_f at $\sqrt{s_{NN}} = 200$GeV is obtained with the help of recent dN/dy data in [41], at all other energies the λ_f data are taken from [40]. It is seen that the theoretical λ_f value increases gradually from ~ 0.5 to ~ 1 fm from AGS to highest RHIC energies with a weak dependence on k_T. The experimental values of λ_f are also between $0.5 - 1$ fm. The observation (both experimentally and theoretically) of a nearly energy independent mean free path on the order of 0.7 fm at pion freeze-out is rather surprising. Physically it has been interpreted as a rather large opaqueness of the pion source at break-up [42, 43].

The HBT duration time "puzzle", i.e. the fact of the theoretical quantity $\sqrt{R_O^2 - R_S^2}$ being larger than extracted from the data, is present at all investigated energies (see Fig. 5 (c)): The calculated values of $\sqrt{R_O^2 - R_S^2}$ are about $3.5 \sim 5$ fm while the measured ones are $1.5 \sim 4$ fm. Many efforts have been put forward over the last years to clarify this issue [39, 44, 38, 46, 45, 28, 27, 25]. Here, we show in Fig. 6 the potential effect on the excitation function of the R_O/R_S ratio at the small k_T. As seen in Fig. 5 (c), the R_O/R_S ratio, which is equivalent to the quantity $\tau \sim \sqrt{R_O^2 - R_S^2}$, is larger than the experimentally observed values at all investigated energies, if the cascade mode (dotted lines with open rectangles) is employed. When the SM-EoS is considered for the formed baryons (solid lines with open diamonds), the R_O/R_S ratio is seen obviously smaller than that with cascade mode and reproduces the (energy dependence of) data at AGS energies. At SPS and RHIC, however, the R_O/R_S ratio is still increasing monotonically with increasing beam energies and deviates from data again. At RHIC energies, the ratio approaches the one with cascade mode. It implies that the potential of formed baryons is increasingly losing its importance with increasing beam energies. At SPS and RHIC energies the deviation from data might be interpreted by the absence of the interactions of unformed particles from string fragmentation. Investigations are in progress.

6. Conclusion and Outlook

To summarize, we show the transverse momentum and beam energy dependence of the HBT radii R_L, R_O, and R_S, the quantity $\sqrt{R_O^2 - R_S^2}$ (and the R_O/R_S ratio), the volume V_f, and the mean free path λ_f of pions at freeze-out for heavy systems with energies from AGS to RHIC. In general, the model calculations with UrQMD v2.2 (cascade mode) are in line with the data over the whole inspected energy range. We also find a nearly constant mean free path for pions on the order of $\lambda_f = 0.7$ fm which indicating a significant opaqueness of the source.

Discrepancies especially in the lower AGS energy region are found and have to be resolved. The HBT duration-time related "puzzle" is present at almost all energies. The consideration of potentials for formed and unformed particles provides new insights into the origin of the time-related puzzle and the dynamics of HICs especially at early stage.

Acknowledgements

We would like to thank the Frankfurt Center for Scientific Computing (CSC). This work is partly supported by GSI, BMBF, DFG and Volkswagenstiftung.

References

[1] T. Matsui and H. Satz, Phys. Lett. B **178** (1986) 416.

[2] S. Soff, S. A. Bass, M. Bleicher, L. Bravina, E. Zabrodin, H. Stöcker and W. Greiner, Phys. Lett. B **471** (1999) 89.

[3] A. Dumitru and R. D. Pisarski, Phys. Lett. B **525** (2002) 95.

[4] U. Heinz and G. Kestin, PoS **CPOD2006** (2006) 038 [arXiv:nucl-th/0612105].

[5] M. A. Lisa, S. Pratt, R. Soltz and U. Wiedemann, Ann. Rev. Nucl. Part. Sci. **55** (2005) 357.

[6] W. Bauer, C. K. Gelbke and S. Pratt, Ann. Rev. Nucl. Part. Sci. **42** (1992) 77.

[7] D. H. Rischke and M. Gyulassy, Nucl. Phys. A **608** (1996) 479.

[8] F. Antinori *et al.* [WA97 Collaboration], J. Phys. G **27** (2001) 2325.

[9] M. A. Lisa *et al.* [E895 Collaboration], Phys. Rev. Lett. **84** (2000) 2798.

[10] L. Ahle *et al.* [E802 Collaboration], Phys. Rev. C **66** (2002) 054906.

[11] S. Kniege *et al.* [NA49 Collaboration], J. Phys. G **30** (2004) S1073.

[12] S. Kniege *et al.* [NA49 Collaboration], AIP Conf. Proc. **828** (2006) 473. [arXiv:nucl-ex/0601024].

[13] D. Adamova *et al.* [CERES collaboration], Nucl. Phys. A **714** (2003) 124.

[14] S. S. Adler *et al.* [PHENIX Collaboration], Phys. Rev. Lett. **93** (2004) 152302.

[15] B. B. Back *et al.* [PHOBOS Collaboration], Phys. Rev. C **73** (2006) 031901.

[16] C. Adler *et al.* [STAR Collaboration], Phys. Rev. Lett. **87** (2001) 082301.

[17] J. Adams *et al.* [STAR Collaboration], Phys. Rev. C **71** (2005) 044906.

[18] K. Adcox *et al.* [PHENIX Collaboration], Phys. Rev. Lett. **88** (2002) 192302.

[19] F. Antinori *et al.* [NA57 Collaboration], J. Phys. G **34** (2007) 403.

[20] S. A. Bass *et al.*, [UrQMD-Collaboration], Prog. Part. Nucl. Phys. **41** (1998) 255.

[21] M. Bleicher *et al.*, [UrQMD-Collaboration], J. Phys. G: Nucl. Part. Phys. **25** (1999) 1859.

[22] E. L. Bratkovskaya *et al.*, Phys. Rev. C **69** (2004) 054907.

[23] S. Pratt *et al.*, Nucl. Phys. A **566** (1994) 103C.

[24] S. Pratt, CRAB version 3, http://www.nscl.msu.edu/ pratt/freecodes/crab/home.html

[25] Q. Li, M. Bleicher, and H. Stöcker, in preparation.

[26] Q. Li, M. Bleicher and H. Stocker, J. Phys. G **34** (2007) 2037.

[27] Q. Li, M. Bleicher, X. Zhu and H. Stöcker, J. Phys. G **34** (2007) 537.

[28] Q. Li, M. Bleicher, and H. Stöcker, Phys. Rev. C **73** (2006) 064908.

[29] J. Aichelin and H. Stöcker, Phys. Lett. B **176** (1986) 14.

[30] J. Aichelin, Phys. Rept. **202** (1991) 233.

[31] H. Sorge, H. Stöcker and W. Greiner, Annals Phys. **192** (1989) 266.

[32] Q. Li, Z. Li, S. Soff, M. Bleicher and H. Stöcker, J. Phys. G **32** (2006) 151.

[33] H. Petersen, Q. Li, X. Zhu and M. Bleicher, Phys. Rev. C **74** (2006) 064908.

[34] M. Isse, A. Ohnishi, N. Otuka, P. K. Sahu and Y. Nara, Phys. Rev. C **72** (2005) 064908.

[35] T. Maruyama, K. Niita, T. Maruyama, S. Chiba, Y. Nakahara and A. Iwamoto, Prog. Theor. Phys. **96** (1996) 263. [arXiv:nucl-th/9601010].

[36] Particle Data Group, D. E. Groom *et al.*, Eur. Phys. J. C **15** (2000) 1.

[37] S. Chapman, P. Scotto and U. W. Heinz, Phys. Rev. Lett. **74** (1995) 4400.

[38] T. J. Humanic, Int. J. Mod. Phys. E **15** (2006) 197.

[39] Z. Lin, C. M. Ko and S. Pal, Phys. Rev. Lett. **89** (2002) 152301.

[40] D. Adamova *et al.* [CERES Collaboration], Phys. Rev. Lett. **90** (2003) 022301.

[41] S. S. Adler *et al.* [PHENIX Collaboration], Phys. Rev. C **69** (2004) 034909.

[42] H. Heiselberg and A. P. Vischer, Eur. Phys. J. C **1** (1998) 593.

[43] B. Tomasik and U. W. Heinz, arXiv:nucl-th/9805016.

[44] J. G. Cramer, G. A. Miller, J. M. S. Wu and J. H. S. Yoon, Phys. Rev. Lett. **94** (2005) 102302.

[45] S. Pratt and D. Schindel, AIP Conf. Proc. **828** (2006) 430.

[46] S. Pratt, Phys. Rev. C **73** (2006) 024901.